Chapter 2 Literature Review

2.1 Preliminary Remark

The fluid flow around single and multiple cylinders of various shapes have captivated scholars over the years. The pioneering investigations of fluid flow around circular cylinder by Sir George Stokes in the 19th century laid the foundation for research on many aspects of fluid flow around cylinders. Since then, development of various methods and tools have been materialized for the study of flow around cylinders. The use of experimental methods (e.g. laser doppler velocimetry, hot-wire anemometry, Particle Image Velocimetry, etc.) and numerical schemes (e.g. large eddy simulation, boundary element method, direct numerical simulation, etc.) for the study of flow around single and multiple cylinders spans several years. However, these methods are expensive and requires significant man-hours. In order to overcome these limitations, researchers are in search of exact analytical solutions of the problem of fluid flow around single and multiple cylinders. There are few exact solutions available with certain assumptions of flow conditions, particularly by neglecting inertial effects (Stokes flow) or by neglecting viscous effects (Potential flow). These analytical solutions build theoretical foundations for understanding fluid flow around cylinders.

In this chapter, the detailed literature review on fluid flow around single and multiple cylinders is carried out. The objective of present chapter is to provide basic understanding of fluid flow behaviour and flow parameters around the cylinders in infinite fluid domain. Also, this chapter details out the investigations on hydrodynamic interaction between the cylinders of different cross-sectional shapes. A brief review of real flow and potential flow around circular and polygonal cylinders using various methods is discussed in below sections.

2.2 Flow around Single Circular Cylinder

Several researchers have investigated the fundamental flow characteristics around circular cylinder. The research articles by Strouhal [2], Morkovin [3], Gerrard [4], Williamson [5] and, monographs by Sumer and Fredsoe [6] and Zdravkovich [7,8] are the notable early contributions.

Among these, the investigations carried out by Wieselsberger [9], Fage and Falkner [10], Roshko [11] and Achenbach [12] have set benchmarks in the field of fluid flow around circular cylinder. The data extracted by these researchers in wide range of flow variables and geometrical parameters provides thorough understanding of flow behaviour around circular cylinder.

2.2.1 Flow Behaviour around a Cylinder

When a cylinder is placed in uniform fluid flow with free stream velocity U_∞ as shown in Figure 2.1, the viscous layer of fluid generates on the surface of cylinder from location of stagnation point on the upstream side of cylinder (at $\theta = 0^0$). This viscous layer of fluid is known as boundary layer. The nature of boundary layer and over all fluid flow behaviour around the cylinder depends on the Reynolds number.

$$Re = \frac{\rho U_\infty D}{\mu}. \tag{2.1}$$

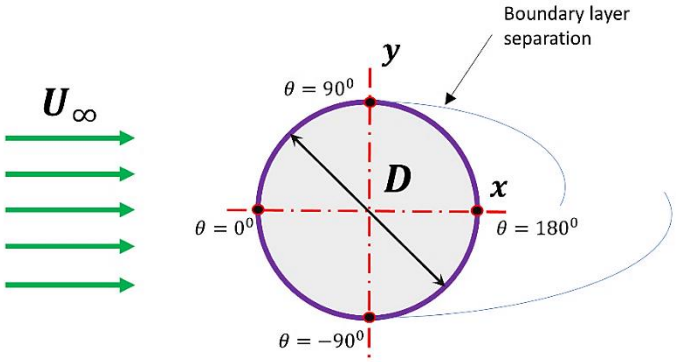

Figure 2.1 Uniform flow around circular cylinder.

At very low Reynolds number ($Re \ll 1$) the viscous effect predominates the flow and the boundary layer of fluid flow remains attached on the surface of cylinder up to the stagnation point on the downstream side of cylinder (at $\theta = 180^0$). Also, the streamlines of flow remain symmetric and follows the shape of cylinder as shown in Figure 2.2 (a) [13].

As the Reynolds number rises, the adverse pressure gradient generates inside the boundary layer. This causes the flow to separate from the surface at two distinct points (separation point) on each side of cylinder. The area behind the cylinder between separation points forms low pressure region

of recirculating flow also known as wake. Inside wake region, the downstream side of cylinder is exposed to negative pressure, while the upstream side of cylinder is exposed to positive pressure, which results in a drag force acting along the direction of flow.

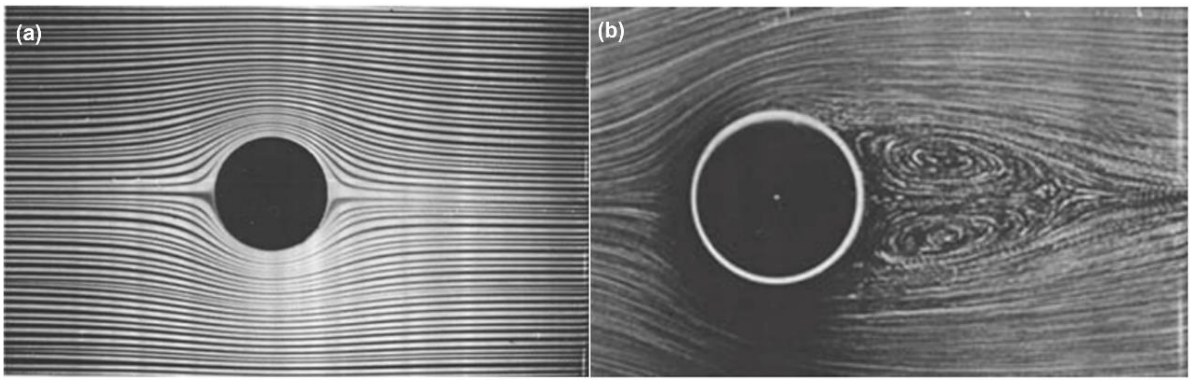

Figure 2.2 Flow around circular Cylinder for (a) $Re \cong 0$ and (b) $Re = 26$ [13].

Further increase of Reynolds number results in increase the size of recirculation zone due to the convection of vorticity from the boundary layer into the wake region from the separation points on each side of the body. At some critical Reynolds number, the recirculation zones become unstable and two vortices starts shedding alternately behind the cylinder from two separation points. This series of alternate vortices is Von-Karman vortex street (Figure 2.3). The formation of Von-Karman street is due to mutual interaction between two separating shear layers from cylinder surfaces [14].

Due to formation of alternate vortices (Von-Karman street) from the separation points, the cylinder experiences lift force normal to flow direction. The magnitude of drag and lift force vary with increase of Reynolds number. Such variation of drag force and lift force co-efficients are shown in Figure 2.4. In plot, $\overline{C_D}$ represents the time-average drag coefficient on the cylinder, that is divided into friction drag $\overline{C_{D_f}}$ and pressure drag $\overline{C_{D_p}}$. As the Reynolds number increases, the transition takes place from laminar to turbulent flow regime and wake behind the cylinder becomes turbulent, this turbulent regime travels upstream up to the free shear layers and finally starts affecting the boundary layers. The turbulent boundary layers contain more kinetic energy, that enable it to resist an adverse pressure gradient. Therefore, the separation point shifts downstream side on the cylinder surface and separation delays. Hence, the wake becomes narrower, that results

in sudden reduction in drag force experienced by the body. This drag drop occurs for $Re = 2 \times 10^5$ on the surface of a smooth cylinder [7]. The effect of roughness on the surface of circular cylinder on the flow behaviour is considered by Fage [15], Achenbach [16], Matteoni and Georgakis [17], Benidir et al. [18], Van Hinsberg [19]. The surface roughness plays an important role in flow transition in boundary layer on the cylinder [16], that can trigger early separation of flow. Due to early separation, the rough surface cylinders experiences more drag as compared to smooth surface cylinder. Many other aspects of flow behaviour around circular cylinder may include effects of ends of cylinder, effect of aspect ratio, effect of yaw angle, etc. Tritton [20], Graf and Yulistiyanto [21], Okamoto and Yagita [22], Parnaudeau et. al. [23], etc. have investigated some of the above aspects of flow around single circular cylinder in subcritical and critical range of Reynolds number.

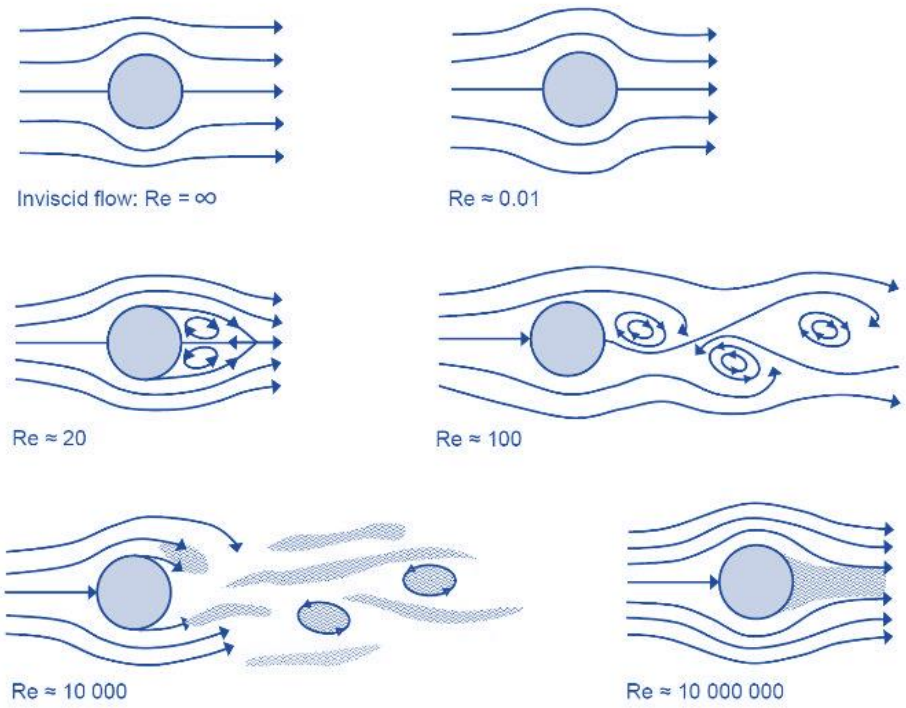

Figure 2.3 Flow around single circular cylinder at various Reynold numbers [24].

At very large Reynold number ($Re \geq 10^7$), the inertia of fluid dominates the flow and the viscous effect can be neglected. Physically the boundary layer of fluid becomes infinitesimally thin on the surface of cylinder and the wake behind the cylinder confines to very narrow region. Such flow at

very large Reynold number ($Re \geq 10^7$) resembles the solutions very close to that for zero viscosity ($Re \cong \infty$). Therefore, the inviscid flow solution at zero viscosity also known as potential flow is a good approximation of flow with very large Reynolds number.

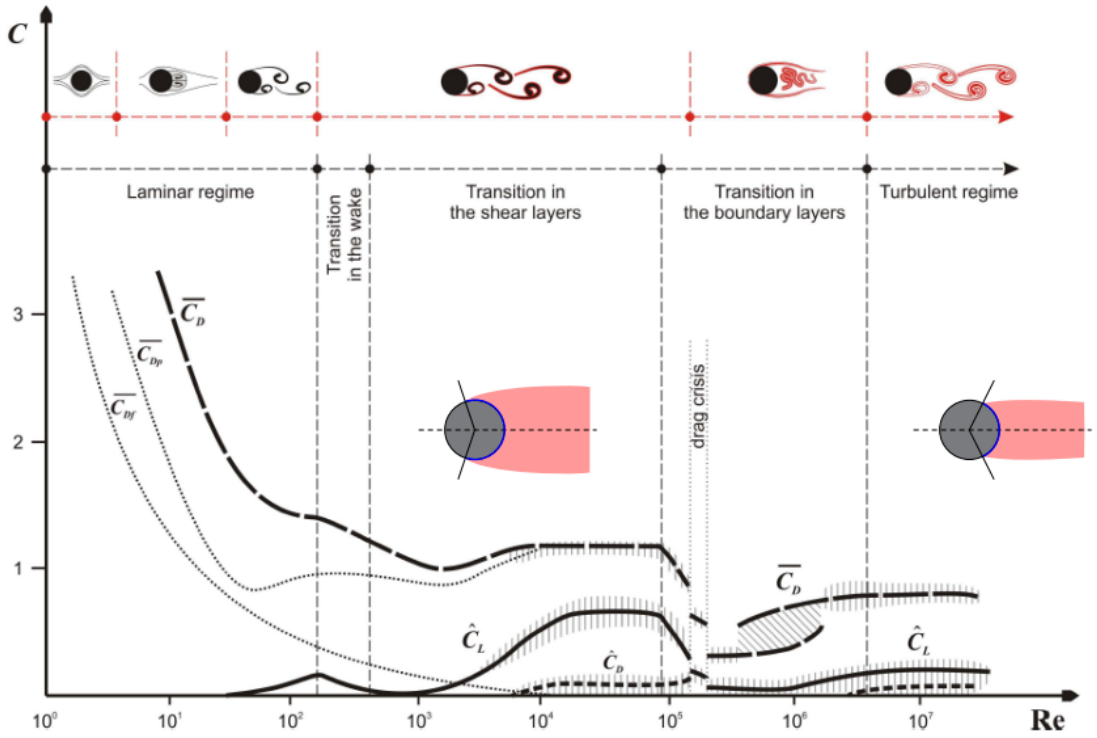

Figure 2.4 Lift force and drag force coefficients variation with respect to Reynolds number for flow on a circular cylinder, dashed regions represent the scatter of experimental data [7].

For large Reynolds number assumption, the Navier-Stokes equation reduces to incompressible Euler equation, which can be further recast in the form of complex potential function $W = \phi + i\psi$, where ϕ and ψ are scalar functions of space known as velocity potential function and stream function respectively. These functions are first introduced by Stokes [25] in 1880. The description of fluid flow in terms of scalar functions that satisfies the Laplace relations ($\nabla^2\phi = 0$, $\nabla^2\psi = 0$) involves the use of complex variable methods.

The potential flow theory based on complex variable method for finding the hydrodynamic parameters around circular cylinders in inviscid incompressible flow is known for more than a century [26–28]. The analytical solution for incompressible uniform potential flow around circular cylinder can be obtained in terms of complex potential function by the principle of superposition.

The superposition of complex potentials for the doublet flow and uniform free stream flow yields the solution for uniform flow around a circular cylinder. The radius of cylinder depends on the strength of doublet and the speed of the uniform flow. The circular cylinder in incompressible uniform potential flow and with no-circulation experiences zero drag and lift force, this is known as D'Alembert paradox. However, the cylinders with circulation (a rotating cylinder) experiences lift force, this phenomenon is known as Magnus effect. The complex potential for a vortex is needed to superimpose with the complex potential for uniform potential flow to include the cylinder rotation effect.

Various cases of potential flow around circular cylinder have been explored by researchers. Yang and Bar-Lev [29] studied impulsively started motion of circular cylinder in potential flow. The inviscid flow separation and vortex formation behind the cylinder is modeled using complex variable method. The inviscid flow around a circular cylinder induced due to free surface travelling waves is explored by Riley and Yan [30]. They derived complex potentials using Perturbation method and numerical solutions are obtained by employing Boundary Element method. The inviscid compressible flow over a circular cylinder has been investigated by Hafez and Wahba [31] by solving complex potential alongwith vorticity and entropy corrections. Botta [32] has studied the inviscid transonic flow around a circular cylinder by numerically integrating the Euler equations using time-dependent technique. The finite difference method is used by Pandolfi and Larocca [33] to explore inviscid compressible flow in transonic range around half and full circular cylinder. Kumar and Salas [34] have considered the problem of compressible potential and viscous flow around a circular cylinder by solving Euler and Navier-Stokes equations respectively using numerical scheme. They observed that with increase in Reynolds number the viscous flow (Navier-Stokes solution) asymptotically approaches to the potential flow (Euler solution) behaviour.

Valentine and Madhi [35] have studied the potential flow around circular cylinder induced by the nearby oscillating disturbances (e.g. pulsating source, pulsating doublet, and pulsating vortex). They have used method of images to model each elementary disturbance around the cylinder and to obtain the hydrodynamic forces acting on cylinder due to oscillating disturbances. The planar potential flow acting on porous circular cylinder is considered by von Wolfersdore and Monch [36], and von Wolfersdore [37]. The nature of potential flow inside a porous cylinder is studied using Darcy's law. Bhattacharya and Raja Sekhar [38] investigated the potential flow around

porous circular cylinder with minor deformation. The effect of thickness of porous material and permeability of porous region on the drag force acting on the cylinder is studied. The shear effect in inviscid flow around circular cylinder is examined by Naguib and Koochesfahani [39]. This work is basically the extension of uniform free stream potential flow around circular cylinder. The schematic of flow around cylinder with linearly varying free stream velocity in cross-stream coordinate is shown in Figure 2.5.

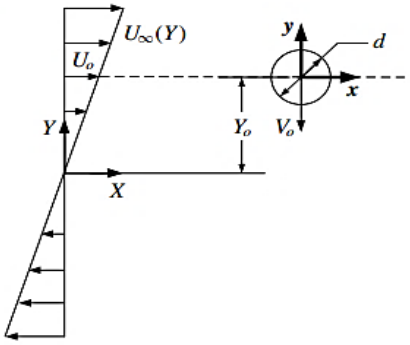

Figure 2.5 Schematic of inviscid shear flow around a moving cylinder [39].

The stream function for the cylinder in inviscid shear flow is given by Tsien [40] as,

$$\psi = U_0\left[\left(r - \frac{d^2}{4r}\right)\sin\theta + \frac{K}{2}\left(\frac{r^2}{d}\sin^2\theta + \frac{d^2}{32r^2}\cos 2\theta\right)\right], \tag{2.1}$$

where, K is a shear rate. For shear rate $K = 0$, the equation of streamline converts to that corresponds to circular cylinder in uniform potential flow. The streamline plots of shear flow around stationary circular cylinder for different values of shear rate K are shown in Figure 2.6.

2.3 Flow around Multiple Circular Cylinders

In engineering applications such as heat exchangers, nuclear fuel rods, cooling fins, etc., the flow is obstructed by multiple cylinders placed in various arrangements. Based on angle α between the direction of flow and line joining centres of cylinders, three types of arrangements are possible for pair of cylinders as shown in Figure 2.7. For angle $\alpha = 0^0$, the cylinders arrangement is known as inline arrangements (tandem configuration), for $\alpha = 90^0$ cylinders show side by side arrangement, and for $\alpha = 45^0$ cylinders assemble in staggered arrangement. Similarly, a group of three cylinders

can arrange in triangular configuration with $\alpha = 30^0$ and $\alpha = 60^0$. More than 3 cylinders forms square (90^0) cluster of inline arranged cylinders or rotated square (45^0) cluster of staggered arranged cylinders (refer Figure 2.7).

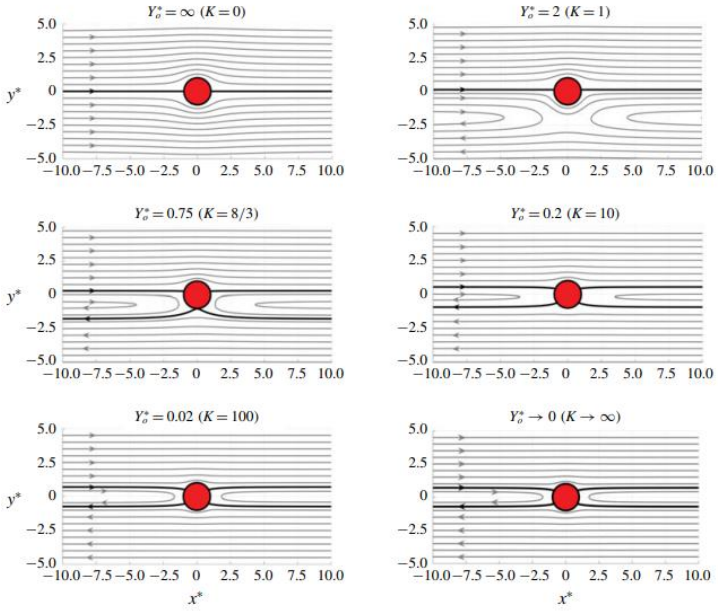

Figure 2.6 Streamlines of the shear potential flow around a stationary circular cylinder [39].

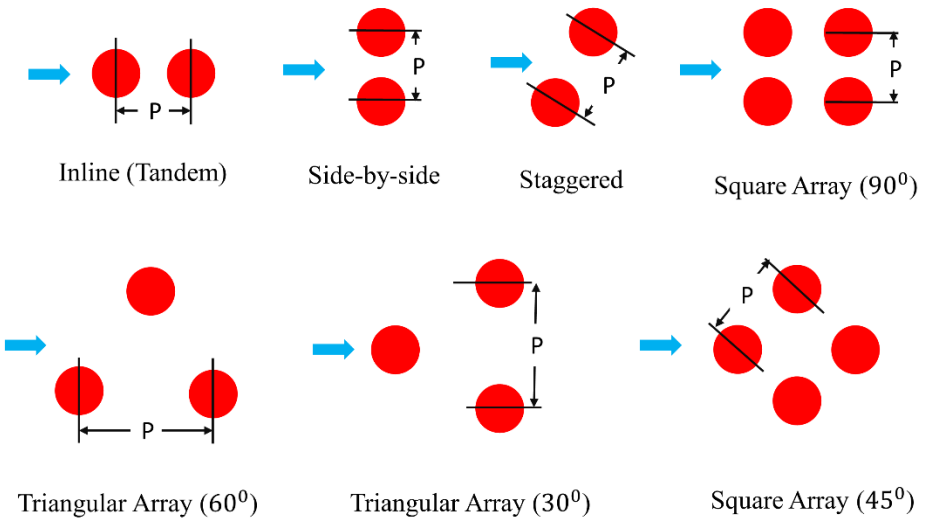

Figure 2.7 Arrangements of group of cylinders in fluid flow.

When these group of cylinders are placed in fluid flow, the fluid flow patterns and flow disturbances generated by one cylinder propagates to the adjacent cylinders and the flow parameters around the cylinders get affected. This type of interaction between the cylinders in fluid is known as hydrodynamic interaction. Hydrodynamic interaction between two bodies can be found in several problems, such as flow over two interacting aerofoils [41–44], the ground effect on an aerofoils lift while take-off and landing of airplanes ([45,46]), marine pipelines near the sea bed [47,48], thermo-wells located close to each other [49], cooling towers [50], transmission lines [51], turbine blades [52], heat exchanger tube bundles [53], etc. The insect flights [54–56], fish schooling [57], birds' flight patterns [58], etc., are some of the examples in nature, where interaction effect is prominent. The hydrodynamic interaction depends on the number of bodies, the arrangement of bodies, spacings between bodies, body shapes, size and their relative orientations.

2.3.1 Hydrodynamic Interaction in Real Flow

The hydrodynamic interaction between two circular cylinders in real fluid flow takes place in three interference regimes [7,59] depending on cylinder spacing, cylinder arrangement, and Reynolds number. These interference regimes are shown in Figure 2.8.

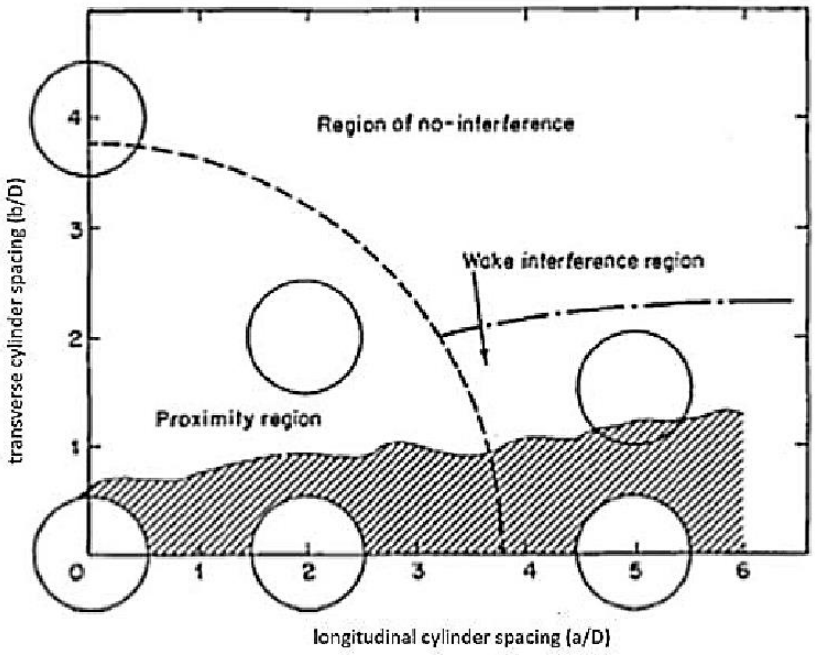

Figure 2.8 Interference regions around the cylinder [59].

1. **Proximity Interference:** The presence of one cylinder affects the flow parameters around other cylinders in close proximity. Proximity interference is proportional to the distance between the cylinders.
2. **Wake Interference:** It occurs when the unsteady wake detaching from upstream cylinder acts on the downstream cylinder. Wake interference is found in tandem and staggered arrangement of cylinders.
3. **Proximity + Wake Interference**: It is region in tandem (inline) arrangement where proximity and wake interference coincide when the downstream cylinder is placed close to the upstream cylinder in the wake region.

Proximity Interference is subdivided into three regimes.

P-SS: side by side arrangement of two cylinders

P-S1: upstream cylinder in staggered arrangement

P-S2: downstream cylinder in staggered arrangement

Wake interference is subdivided into two regimes.

W-T: tandem wake interference

W-S: staggered wake interference

P-SS: Side by side arrangement

In side by side arrangement (for flow angle $\alpha = 90^0$) three flow regimes are observed in subcritical range of Reynolds number ($10^4 \leq Re \leq 10^5$) as shown in Figure 2.9 [60]. The characteristics of these regions are discussed in Table 2.1. For center-to-center distance between the cylinders to diameter ratio (H/D) ranging 1 to 1.2, single street of vortices formed behind both the cylinders. For H/D ratio ranging 1.2 to 2.2, the gap flow between two cylinders forms a bi-stable biased jet, that switches towards the narrow and wide wake of two cylinders at irregular time interval. Bearman & Wadcock [61] observed huge difference in the drag forces experienced by cylinders with narrow and wide wake. The value of flow angle 'α' greater or less than 90^0 results in permanently biased flow towards one of the cylinders. For $2.7 < H/D < 5$, the identical wake

forms behind both cylinders and for spacing $H/D > 4$, the wake behind both cylinders behaves independently and does not show hydrodynamic interaction effects.

Table 2.1 Excitation Regions in side by side arrangement of cylinders

Designation	*Region*	*Characteristics*
P-SSA	1<H/D<1.2	▪ Unit Vortex Street is formed around the cylinders with bleed through gap.
P-SSB	1.2< H /D<2.2	▪ Narrow and wide wake formed around identical cylinders ▪ Flow through gap between the cylinders forms a jet biased towards narrow wake which is bi-stable. ▪ Jet switches in opposite direction at intermittent time interval, narrow and wide wake interchange behind the cylinders.
P-SSC	2.7< H /D<5	▪ Both near wakes are equal in size, coupled and mirror of each other ▪ Both vortex shedding is harmonized in phase and frequency.

P-S1 and P-S2 Staggered Arrangement

In *P-S1* and *P-S2* regimes, the cylinders are placed in staggered arrangement in proximity to each other as shown in Figure 2.9. In these configurations, the upstream cylinder forms narrow wake as compare to downstream cylinder and it experience positive lift with small decrease in drag for flow angle $\alpha > 40^0$.

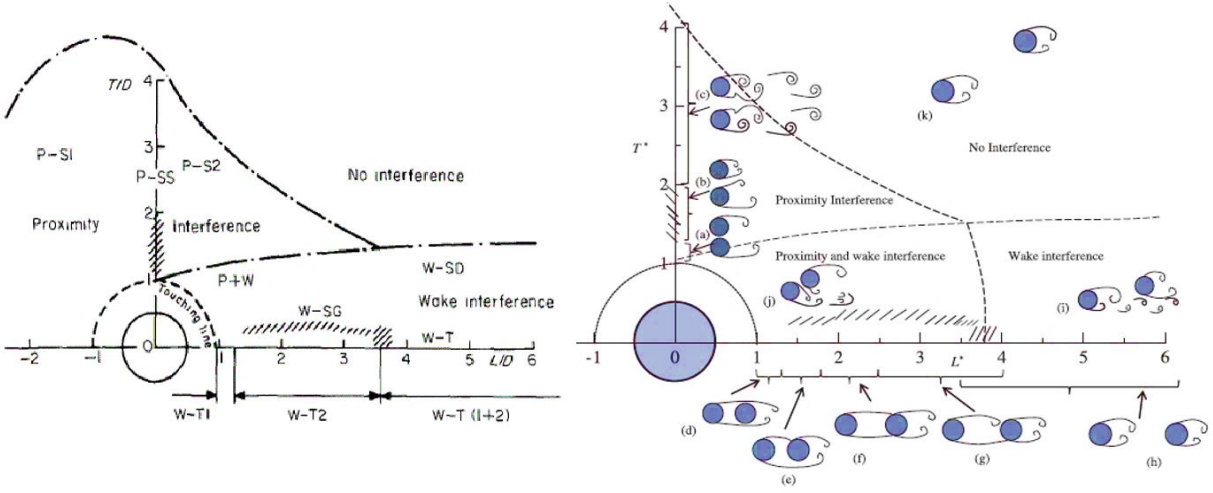

Figure 2.9 Interference flow regimes for side-by-side, tandem and staggered arrangements of two pipes [7,62].

W-T: Tandem Wake Interference

In tandem configuration for the flow parallel to the line connecting the centres of cylinders, the spacing between the cylinders is denoted as L/D. Various wake interference regimes exist in tandem arrangements of cylinders [60]. These regimes are sub classified and described below.

W-T1: for $1 < L/D < 1.8$, the vortex street behind downstream cylinder is formed by free shear layer detaching from upstream cylinder.

W-T2: for $1.8 < L/D < 3.8$, Boundary layer detaching from upstream cylinder reattach on downstream cylinder's front side. Unit vortex street is formed around downstream cylinder.

W-T (1+2): for $L/D > 3.8$, Separating shear layer forms the vortex street on both upstream and downstream cylinder. Vortex Street shedding from downstream cylinder is known as binary vortex street as it consists two vortex street formed from upstream and downstream cylinder.

W-S: Staggered Wake Interference

Staggered wake interference regimes exist when the downstream cylinder is placed in the wake of upstream cylinder in staggered form. These regimes are subclassified as discussed below.

W-SG (Gap Flow): for horizontal spacing 1.1 to 3.5 and vertical spacing 0.2, the gap flow between cylinders induced lift on both cylinders, which vanishes for vertical spacing less then 0.2 as gap flow ceased.

W-SD (Wake Displacement): for horizontal spacing more than 2.8 and vertical spacing more than 0.4, the displacement of wake behind upstream cylinder generate lift force on downstream cylinder. The lift force acting on downstream cylinder is found maximum in wake region boundaries and reaches to zero as tandem arrangement is reached.

In wake interference regime, the cylinder commonly experiences periodic excitation forces and that results in vibratory motion of cylinders known as flow induced vibration (wake induced galloping). Similarly, when cylinder is placed in proximity+wake interference regime, the cylinders experiences the excitation forces as a combined effect of both proximity and wake interreference. In the absence of wake in potential flow, the cylinders only experience steady hydrodynamic loads due to proximity interferences.

2.3.2 Hydrodynamic Interaction between Circular Cylinders in Potential Flow

The flow visualization and the experimental work performed by Mavriplis [63] and Wallis [64] showed that wake behind the cylinders supresses and becomes narrower when cylinders are placed in groups in close proximity as shown in Figure 2.10. The cylinders in groups causes the fluid to deflect into the wake regions and the separation bubbles behind the cylinders are confined to small areas. These situations caused the flow patterns similar as potential flow around multiple cylinders. Therefore, the potential flow solution around the cylinders can be adopted by considering the entire flow region inviscid and irrotational for very large Reynolds number (theoretically $Re \cong \infty$). In potential flow around the multiple cylinders, the proximity is the only interference regime that is present due to absence of wake behind the cylinder.

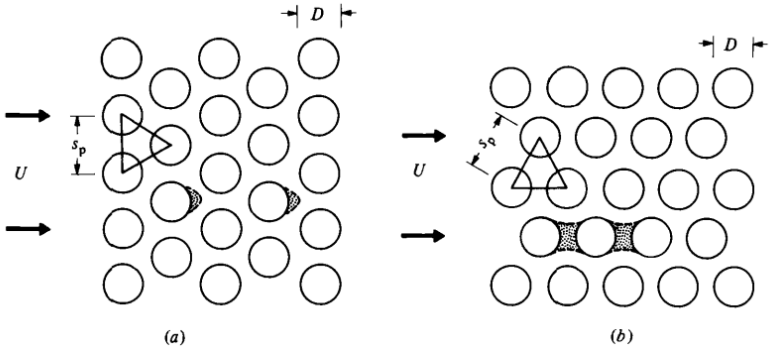

Figure 2.10 Flow patterns around cylinders array (a) Triangular (30^0) (b) Rotated Triangular (60^0) [65].

The potential flow approach to obtain the analytical solution of flow around multiple circular cylinders is attempted by many researchers. Most of the earlier studies of potential flow in doubly connected domain are limited to simple geometries such as spheres and circular cylinders due to complex mathematical treatment involved. Hicks [66], Basset [67], Herman [68], Lamb [69], Rouse [70], Bentwich and Miloh [71], Sun and Chwang [72], etc. have studied hydrodynamic interaction between two spheres in potential flow.

The problem of uniform potential flow over two parallel circular cylinders is addressed by Hicks [73] using definite integrals associated with complex velocity potential function. Greenhill [74] and Carpenter [75] have provided the series solution for potential flow over two circular cylinders. Huang and Yong [76], Alassar and Ei-Gebeily [77], and Chen et al. [78] obtained the solution for potential flow around two circular cylinders using bipolar co-ordinates. Lagally [79] developed the complex potential function for flow past two-cylinders using Weierstrass function.

The potential flow due to a line source and sink around two stationary circular cylinders is studied by Ahammad and Sen [80] using Earnshaw stream function. The forces and torque acting on the cylinders due to hydrodynamic interaction are derived for various center distances. Taylor [81] investigated behaviour of two circular cylinders interacting hydrodynamically in inviscid oscillatory flow with low Keulegan Carpenter number ranging from 2 to 10. In oscillatory flow, the non-dimensional Keulegan Carpenter number relates the drag force and inertia force acting on a body. The effect of spacing between the cylinders and the ratio of radii of cylinders on the hydrodynamic interaction is considered (Figure 2.11).

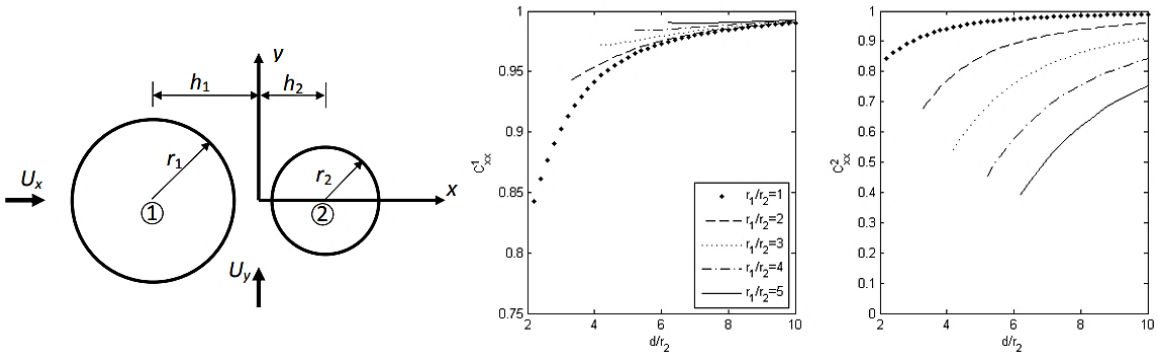

Figure 2.11 (Left) Geometry, (Right) Force co-efficients acting on cylinders for different ratio of radii [81].

The complex velocity potentials for two translating and expanding circular cylinders in uniform potential flow are developed by Wang [82] using conformal mapping and Fourier series expansion. For very large center-to-center distance, the hydrodynamic interaction between cylinders weakens and the solution reduces to that for single circular cylinder moving in potential flow. The force acting along the line connecting the centers of cylinders is inversely proportional to the center distance, whereas those acting normal to the center line are inversely proportional to the square of the center distance. For one expanding and other contracting cylinder, the hydrodynamic force acting between the cylinders is of attractive type in nature. For both expanding or contracting cylinders, the repelling force acts between them. The hydrodynamic coupling between circular cylinders moving along the line connecting cylinder centers is presented by Borisov et al. [83].

For two moving circular discs in inviscid flow, the complex potentials in terms of first Jacobi theta function are derived by Burton et al. [84]. They used Mobius transformation to map flow from annulus to the flow around two circular disc. The first order poles in an annulus are mapped to the

vortices outside two discs, and second order poles in annulus corresponds to uniform flow at infinity around two circular discs.

The method of images is used by Kawaguti [85] to model potential flow past two cylinders. Also, Bampalas and Graham [86] adopted bilinear mapping [87] as shown in Figure 2.12 to investigate the forces between two unequal circular cylinders in inviscid flow.

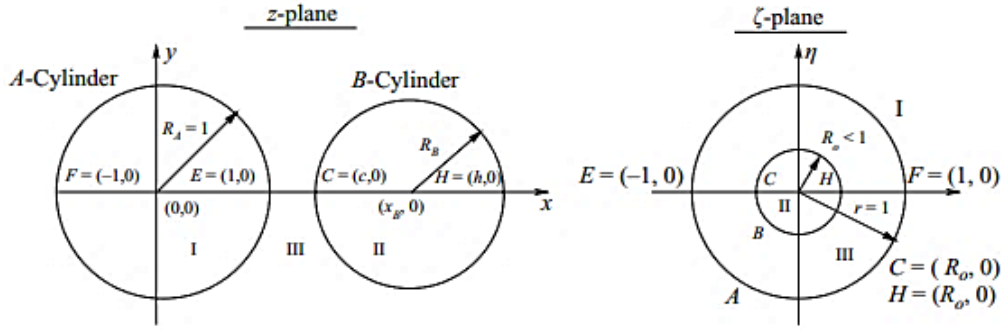

Figure 2.12 Bilinear transformation from annulus region to the region outside two circles [86].

Gao et al. [88] investigated the flow past two circular cylinders in tandem arrangement by studying the streamlines of potential flow. From the streamlines between two unequal circular cylinders, the wake transition from the behaviour of single bluff body to the alternate reattachment is studied and threshold condition for that is obtained. Such threshold condition is function of ratio of diameters of cylinders, non-dimensional distance between cylinders, and uniform flow speed. Figure 2.13 shows the nearest streamline around the surface of cylinders for different center distance to diameter ratios (H/D). For center distance H/D = 1.43, the streamlines cut the gap between the two cylinders diagonally and cross the axis joining the cylinder centers, this indicates transition from single bluff body behaviour to the alternate shear layer reattachment behaviour.

For infinite diameter of one of the circular cylinders, the problem of flow around two-circular cylinders is transformed to the flow around cylinder near a wall/ground. The hydrodynamic interaction between the circular cylinder and plane wall is investigated by Petrov and Maklakov [89] using potential flow theory. They have constructed the complex potential function using Jacobi Theta-functions and the circulation around the circular cylinder is determine using Gol'dshtik's principle. Baddoo and Ayton [45] gave the exact solution for ground effect on circular cylinder in potential flow using complex potential function for doubly connected annulus domain.

They proposed the solution in two steps, in first step the complex potential function inside an annulus domain is developed and, in second step the conformal mapping from doubly connected annulus domain to the physical domain of interest is constructed.

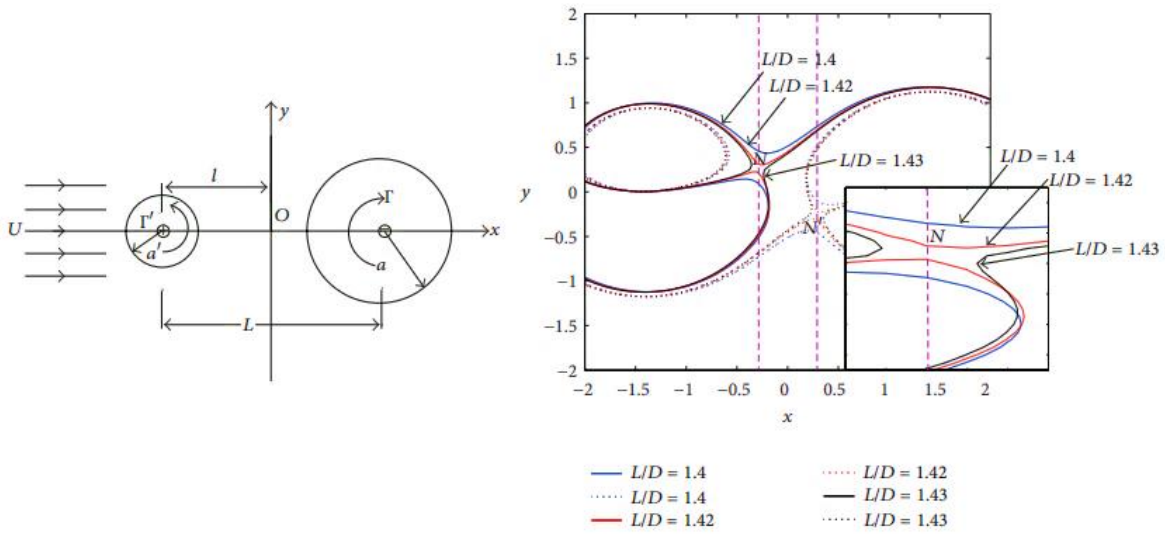

Figure 2.13 (left) Two different diameter circular cylinders in tandem arrangement, (right) The enlarged view of streamlines on surface of cylinders for different *L*/*D* [88].

The potential flow around multiple circular cylinders is studied by Dalton and Helfinstine [90] by extending the method of images to the multiply connected domain. Crowdy [91] used Mobius transformation for multiply connected region to investigate flow around circular cylinders in tandem and side by side configurations with and without circulations. The series solution of potential flow around multiple circular cylinders is developed by DeLillo et al. [92]. Sun and Ng [93] studied the hydrodynamic interaction between multiple translating cylinders in inviscid fluid using complex potential function in form of power series. Paidoussis, Price and Marviplis [94] gave semi analytical model for vibrating cylinders in an array placed in cross flow using superposition of the empirical and potential flow solution. The stability of cylinders in cross is studied and threshold of fluid elastic instability is predicted.

Lagrange et al. [95] have developed the analytical method for determination of added mass of two unequal circular cylinders interacting in potential flow. The exact analytical expressions for finding of fluid added mass coefficients are proposed. They observed that, the self-added mass decreases with increase of center-to-center distance and increase with the increase of ratio of

diameters. The translation of cylinders along the center line towards each other induced repulsive forces between the them. For the case of one stationary cylinder and second vibrating, the forces imposed on stationary cylinder in the opposite direction of displacement of vibrating cylinder, whereas the force on the vibrating cylinder acts in same direction of displacement.

2.4 Flow around Single Polygonal Cylinder

Polygons are closed loop geometries formed by connection of finite number of line segments which forms edges/sides of polygons. Depending on number of sides and inclusion angles, the polygonal geometries are mainly classified into regular and irregular type. The polygons with equal length of all sides and equal inclusion angles are known as regular polygons. Polygons with different length of sides and inclusion angles are known as irregular polygons. Each interior angle of a regular polygon is given by formula $[(2N-4) \times 90°]/N$, and the sum of all inclusion angles of polygon can be obtained from formula $(N-2) \times 180^{0}$, where N represents number of sides of polygons.

The polygonal geometries of various shapes, size and orientations can be generated using conformal transformations in complex variable methods. The polygons with sharp corners and straight sides can be mapped from circles with the help of Schwarz–Christoffel transformation [96]. The conformal transformation can be formulated using parametric equations of hypotrochoid. The close geometry with N number of such hypotrochoids forms a polygon with rounded corners and curved sides [97,98].

2.4.1 Polygonal Cylinder in real flow

In practice, structural/mechanical members with different cross-sections are utilize to cater certain purposes e.g. drag reduction, suppression of flow induced vibration, passive flow control, augmentation of convective heat transfer, etc.

The flow past regular and irregular polygonal geometries have been studied by researchers with different objectives (e.g. triangular [99–101], rectangular [102,103], hexagonal [104,105], trapezoidal [106], diamond [107], and N sided polygons [108,109]). Jackson [110] investigated the periodic behaviour of two-dimensional laminar flow around flat plate, and cylinder of circular, elliptical and triangular section using finite element simulation. The critical Reynolds number and

corresponding values of Strouhal number are calculated for the onset of periodicity of flow around a cylinder. Zhu et al. [111] have studied the flow around trapezoidal cylinder of different base length ratio ranging 0 to 1 as shown in Figure 2.14. It is observed that the hydrodynamic forces acting on cylinders increase significantly as flow angle changes from 0° to 180°. For all configurations the pressure attains the maxima at the midpoint of the front base, and it decreases attains minima at vertices where flow separation occurs.

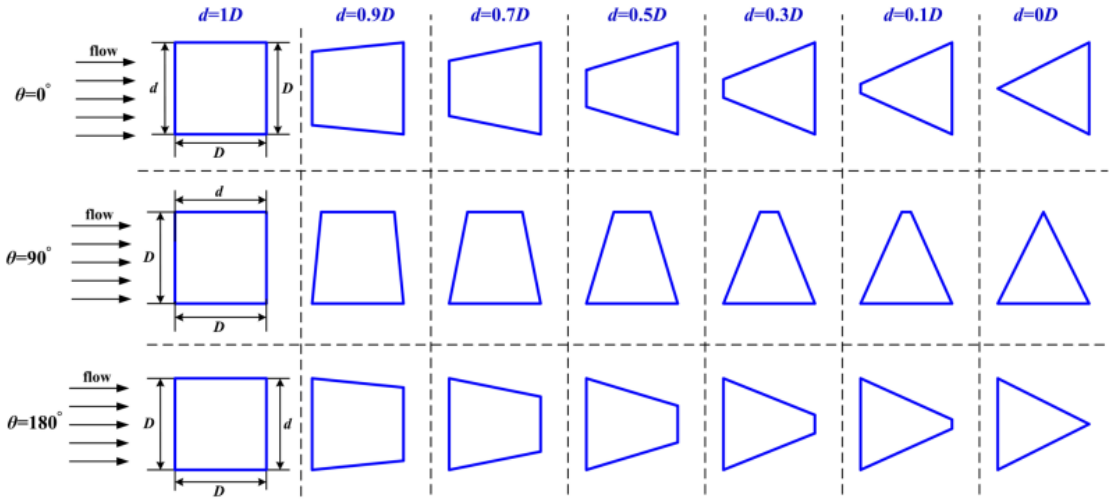

Figure 2.14 Trapezoidal cylinders of different base length ratio and orientations [111].

Tian and Li [112] studied aerodynamic behaviour of polygonal cylinder of number of sides $N = 24$ in low speed wind tunnel. The purpose of their study is to install prototype supporting frames in wind tunnel with low drag force. They obtained 40 % drag reduction with instalment of polygonal section frame as compared to that for circular section frame. An octagonal tapered cylinder subjected to the fluid flow of Reynolds number ranging between $3 \times 10^3 \leq Re \leq 2 \times 10^4$ is studied by Bosch and Guterres [113]. They found lower drag force for side facing the flow as compared to that for corner facing the flow. It is observed by Deniz and Staubli [114] in their experiment of flow around rectangular and octagonal cylinders that the energy transmission from fluid to cylinder is closely related to the phase difference between fluctuating lift force and oscillating cylinder.

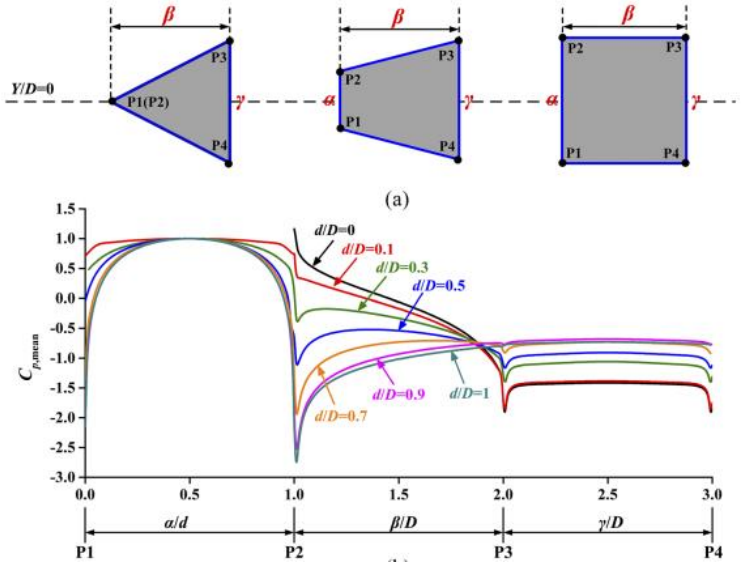

Figure 2.15 The pressure coefficients on the surface of trapezoidal cylinder [111].

The flow behaviour on the surface of polygonal cylinder of sides $N = 5$ to 8 is investigated by Masoudi et al. [115] and Masoudi et al. [116] using large eddy simulation. They tested polygonal cylinder for six different flow angles ranging from flow facing side to flow facing corner at Reynolds number $Re = 10^4$. Their study involved computation of lift force, drag force and vortex shedding frequencies behind the cylinder. The complex dependency of these flow parameters on flow angle and number of sides of polygon is observed. The pressure co-efficient profile on the surface of polygonal cylinder with $N = 5,6,7$ and 8 are shown in Figure 2.16. Pressure changes abruptly at the corners of polygons, and maximum pressure drop is reported at the primary separation point. The insignificant pressure drop is observed at the corners in the separation region.

The flat plate, triangular, square, pentagonal, and hexagonal cylinder to the N-sided polygonal cylinders are examined by Xu et al. [117] for leading corner/flat surface facing the free stream flow with Reynolds number $10^4 \leq Re \leq 10^5$. In their study, it is observed that the lift and drag forces acting on cylinder varies with number of sides N of cylinder. For small values of N, drag co-efficient varies greatly between corner facing and side facing orientation of cylinder. The variation of drag force between side facing and corner facing orientation reduces as N becomes large. The lift co-efficient is found to be increases with increase of number of sides N and drops before attaining the values that corresponds to circular cylinder (for $N = \infty$).

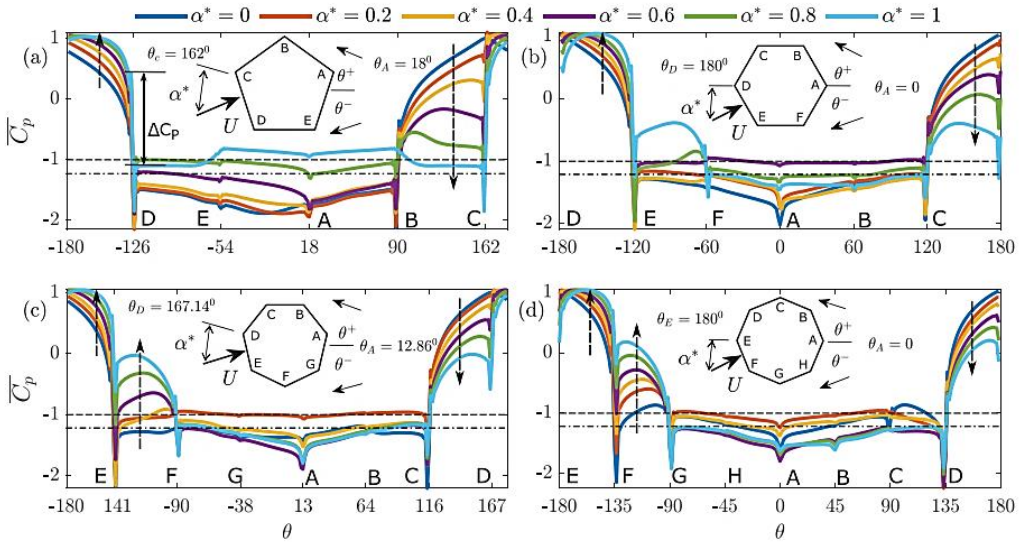

Figure 2.16 Pressure distribution on the periphery of polygonal cylinder [115].

Orlando et al. [118] studied the aerodynamic properties of 16-sided polygonal cylinder with imperfection and ancillaries. They have considered two polygonal cylinders with certain peculiarities, e.g. round corners, protuberance due to weld bead, cable, duct and external ladder attached with cylinder. The effects of such peculiarities on the hydrodynamic load on cylinder and other flow parameters are investigated, and also checked for sensitivity of galloping instability.

Wang et al. [119] have studied the wake behind the polygonal cylinder of side number $N = 3$ to ∞ at $Re = 1.6 \times 10^4$. The vortex evolution in the wake of cylinder is investigated using proper orthogonal decomposition. The behaviour of fluid flow (mean velocity, wake width, vortex formation length, etc.) in wake of polygonal cylinder is significantly affected by number of sided N and cylinder orientation.

The flow behaviour and heat transfer characteristics around square cylinder with rounded corners is studied using numerical method at Reynolds number $Re = 150$ for corner radii 0 (square), $0.125, 0.25, 0.375,$ and 0.5 (circular) by Zafar and Alam [120]. It is found that pressure co-efficient attains maxima at front stagnation point ($\theta = 0^0$), and it decreases with increase of corner radii on the surface between $0^0 < \theta < 35^0$ (front surface). Very large pressure drop occurs at the vertex of square due to flow separation, the pressure at this point increases with increase of corner radii. Also, between $45^0 < \theta < 135^0$ (side surface) the pressure recovers and maintain

constant value in the range $135^0 < \theta < 180^0$ (rear surface). The base pressure co-efficient attains maxima and minima for corner radius 0.125 and 0.5 respectively.

The fluid flow around N sided isotoxal-star shaped polygonal cylinder is studied by Lee et al. [121] in uniform flow of low Reynolds number $Re = 150$. Isotoxal polygonal cylinders are regular N sided cylinders with N number of V-grooves as shown in Figure 2.17. To investigate the effect of V-groove on the hydrodynamic forces acting on the cylinder, the transformation of polygonal cylinder in step-by-step manner is considered, which allows the study of effect of addition of each groove in cylinder. The separation points on cylinder shift with addition of number of grooves as shown in Figure 2.17for configuration with 4 grooves/vertices and side flow facing.

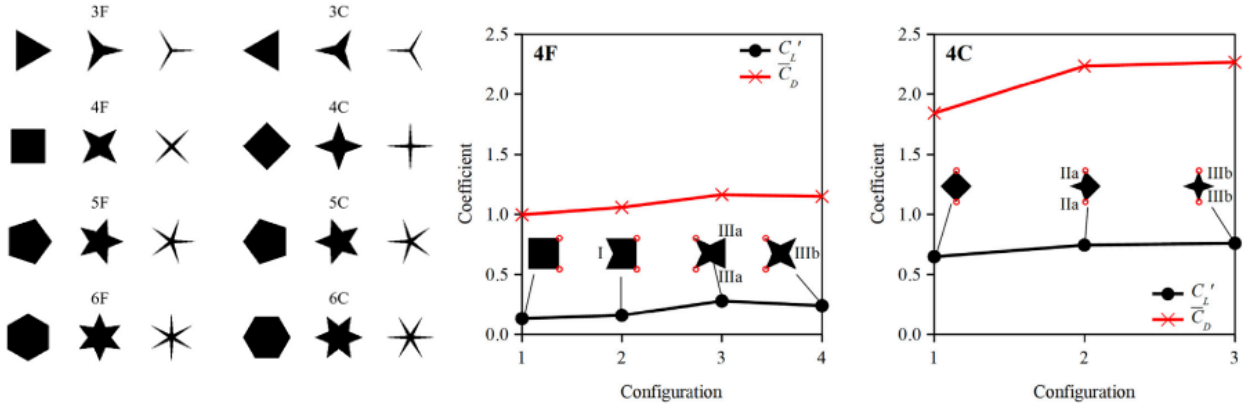

Figure 2.17 Regular polygonal and isotoxal-star polygonal cylinder (left), force co-efficients on polygonal cylinder for N=4 (Right) [121].

Park and Wang [122] have studied the behaviour of floating polygonal platforms placed inside a polygonal ring in waves. The case of polygonal platform and surrounding ring oscillating together and the case of individual oscillation of platform and ring are considered. The hydrodynamic interactions among the floating polygonal platform, surrounding ring and trapped waves are investigated. The effect of radii of platform and ring, and the shape of platform on the hydrodynamic parameters such as hydrodynamic forces, added mass, radiation damping and wave field have been explored.

Scolan and Etienne [123] have proposed the method to calculate the hydrodynamic forces acting on the body of arbitrary shapes in viscous fluid flow. They have projected the Navier Stokes

equation on sets of functions with the help of method developed by Quartapelle and Napolitano [124], these functions are associated with potential flow theory. The results are presented for rectangular section; the rectangular shape is obtained by combination of Karmann–Trefftz transformation and Theodorsen–Garrick transformation as shown in Figure 2.18.

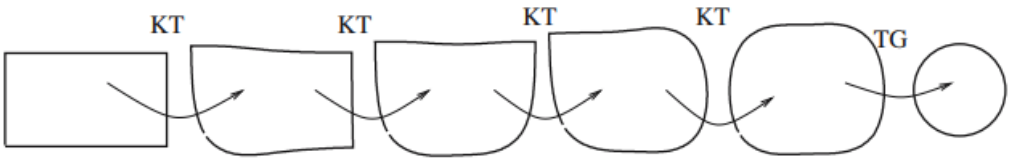

Figure 2.18 Conformal transformations from a rectangular shape to a unit circle using combination of Karmann–Trefftz and Theodorsen–Garrick transformation [124].

2.4.2 Single Polygonal Cylinder in Potential Flow

The complex variable methods along with conformal mappings into potential flow theory can be used to study the behaviour of flat plates [125], aerofoils [126] and other complex shaped geometries in fluid flow. Some of the earlier studies of potential flow over noncircular geometries have involved the use of Joukowsky [127] and Schwarz-Christoffel [96] transformation to map the region outside of a circle to outside aerofoils and polygonal geometries respectively.

Tian and Wu [128] used Schwarz-Christoffel mapping for the investigation of inviscid flow and viscid flow (low Reynolds number $Re < 200$) around a polygonal cylinder with even number of flat edges (N) and one of the vertices facing the free stream. They showed that, in inviscid flow the pressure-drop around the vertices of polygonal cylinder is inversely proportional to the number of sides (N) of polygonal cylinder. The low-pressure region around vertices is shown by a circle in Figure 2.19. The radius of this circle representing low-pressure region decreases with increase of number of sides N of cylinder. Tian et al. [129] have further considered the flow around polygonal cylinder with odd number of edges and different orientations. It is shown that the low-pressure region expands as apices moves towards centreline in contour plots (Figure 2.20). They have also shown the behaviour of first critical Reynolds number at which the separation of flow starts when polygonal cylinder is placed in viscous flow. There is decrement of critical Reynolds number with increase of number of sides of cylinder.

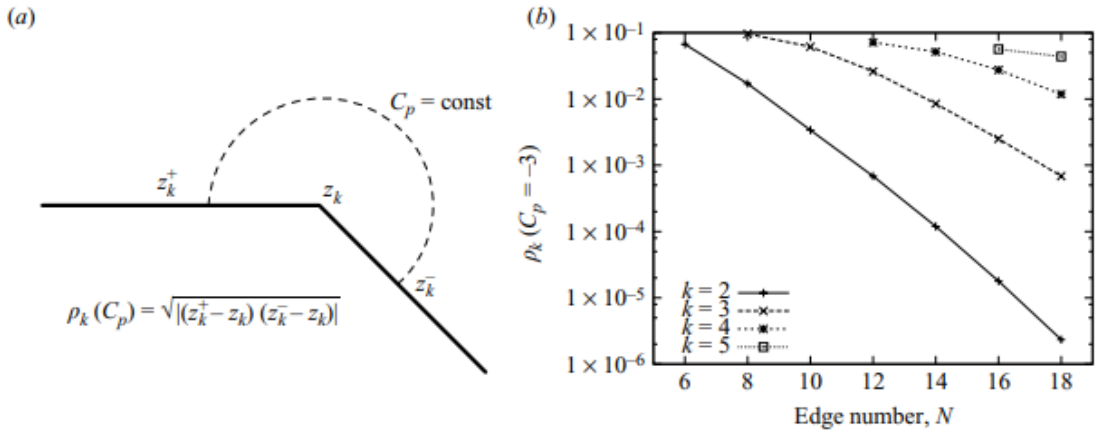

Figure 2.19 Low-pressure region radius of apices on polygon surfaces [128].

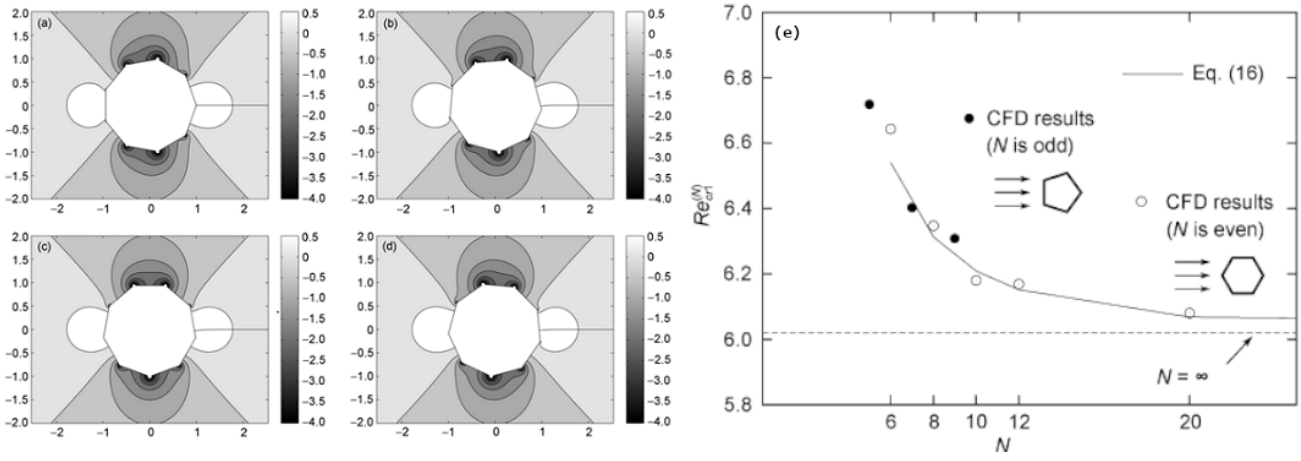

Figure 2.20 Pressure contours around polygon cylinder ($N = 9$) in uniform potential flow, where cylinder orientation γ varies from 0 to γ/N (a) γ = 0°, (b) γ =5°, (c) γ =10°, (d) γ = 20° and, (e) variation of first critical Reynolds number with respect to N in viscous flow [129].

Using Schwartz-Christoffel transformation, Morishita [130] has investigated the potential flow around regular polygonal cylinders of sharp corners and straight sides for $N = 3, 4$ and 6. In their study, the pressure co-efficient on the surface of triangular, diamond and square shaped cylinder are obtained as shown in Figure 2.21. It is found that maximum absolute values of velocity and pressure co-efficient at the middle of shoulder increases with increase of N and attain the values corresponding to circular cylinder for very large value of N.

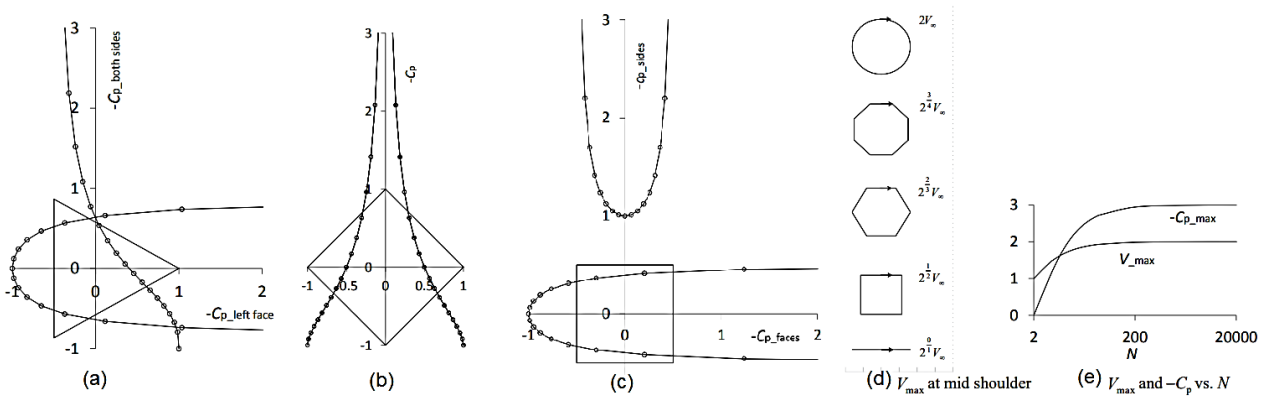

Figure 2.21 Pressure co-efficient Cp on the surface of (a) triangular, (b) diamond and (c) square shaped cylinder and, (d) V_{max} at mid shoulder and (e) V_{max} and Cp vs. N [130].

Elcrat and Trefethen [131] have used modified Schwarz-Christoffel integral to compute Kirchhoff flow (ideal incompressible flow around an object with still wake bounded behind it by free streamlines) around arbitrary polygonal obstacle. In their method, the parameters associated with Schwarz-Christoffel integral are handled using numerical method developed by Trefethen for Schwarz-Christoffel map. The rotational flow past a polygonal cylinder is studied by Sarma [132]. The hydrodynamic forces acted on polygonal cylinder are calculated, and found that they are independent of number of sides of polygonal cylinder. Kim and Kim [133] gave approximate analytical solution for potential flow around square cylinder using higher order multipoles. For investigation of an inviscid uniform shear flow past a smooth concave body, circular arc and Kidney shaped body, the stream function is derived by Murad [134] using complex variable method. The data of various cylinder geometries, flow conditions and the methods considered by researchers are summarized in Table 2.2 for flow around single cylinder and in Table 2.3 for flow around pair of cylinders.

2.5 Flow around Multiple Polygonal Cylinders

Hydrodynamic interactions between the members of polygonal cross sections are found in some of the specific applications like floating polygonal platforms [122,135], piers of bridges interacting in cross flow [136,137], tubes in heat exchangers [53,138], etc. The investigations on the hydrodynamic interactions between multiple polygonal cylinders carried out by some of the researchers are discussed below.

Table 2.2 Various types of cylinder geometry, flow conditions and investigation methods used by researcher for flow around single cylinder

Researcher	**Cylinder Geometry**	**Flow condition**	**Method Used**
Strouhal [2], Morkovin [3], Gerrard [4]	Circular cylinder	Real flow	Experimental
Stringer et al. [139], Catalano et al. [140]	Circular cylinder	Real flow	Numerical Simulation (URANS)
Travin et al. [141]	Circular cylinder	Real flow	Detached Eddy Simulation
Lu and Dalton [142]	Circular cylinder	Real flow	Large Eddy Simulation
Mustto et al. [143]	Circular cylinder	Real flow	Discrete Vortex Method Simulation
Kostecki [144]	Circular cylinder	Real flow	Random Vortex Method Simulation
Dong and Karniadakis [145]	Circular cylinder	Real flow	Direct Numerical Simulation
Hafez and Wahba [31]	Circular cylinder	Inviscid compressible flow	Complex variable
Botta [32]	Circular cylinder	Inviscid transonic flow	Numerically integrating the Euler equations
Pandolfi and Larocca [33]	Circular cylinder	Inviscid compressible flow	Finite-difference method
Kumar and Salas [34]	Circular cylinder	Compressible potential and viscous flow	Numerical scheme
Valentine and Madhi [35]	Circular cylinder	Potential flow induced by oscillating disturbances	Method of Images and Boundary Integral Method
Yang and Bar-Lev [29]	Circular cylinder	Potential flow on Impulsively started cylinder	Complex variable method
Riley and Yan [30]	Circular cylinder	Potential flow induced by travelling of free surface waves	Perturbation Method and Boundary Element Method
von Wolfersdore and Monch [36] and von Wolfersdore [37]	Porous circular cylinder	Potential flow	Complex variable method
Bhattacharya and Raja Sekhar [38]	Porous circular cylinder with minor deformation	Potential flow	Complex variable method
Naguib and Koochesfahani [39]	Circular cylinder	Inviscid shear flow	Analytical method
Tsien [40]	Circular cylinder	Inviscid shear flow	Complex variable method
Mushtaq et al. [146]	Elliptical Cylinder	Potential Flow	Boundary Element Method
De and Dalal [99]	Triangular cylinder	Two-dimensional laminar viscous flow	Finite volume method
Agrwal, Dutta, and Gandhi [100]	Triangular cylinder	Real flow	Experimental Method
Liu et al. [101]	Triangular cylinder	Real flow	Numerical Simulation

Sohankar et al. [102]	Rectangular	Two-dimensional and Three-dimensional unsteady flow	Implicit fractional step method finite-volume code
Mashhadi et al. [103]	Rectangular	Two- and three-dimensional unconfined flows	Numerical Simulation
Ghosh et al. [104]	Hexagonal	Real flow	Experimental Method
Karampour [105]	Hexagonal and Textured cylinder	Real flow	Numerical Simulation
Dhiman [106]	Trapezoidal	Non-Newtonian power-law fluid flow (Shear-thinning and shear-thickening fluids)	Numerical Simulation
Jiang [107]	Diamond	Three-dimensional	Direct numerical simulations (DNS)
Dey and Das [108]	triangular thorn attached to square cylinder	Real flow	Numerical Simulation
Alam et al. [109]	Square cylinder with variable corner radii	Real flow	Numerical Simulation
Jackson [110]	Flat plate, circular, elliptical and triangular cylinder	Real flow	Finite-element simulations
Zhu et al. [111]	Trapezoidal cylinder of different base length ratio	Real flow	Numerical Simulation
Tian and Li [112]	Polygonal cylinder of number of sides $N = 24$	Real flow	Experimental method
Bosch and Guterres [113]	Octagonal tapered cylinder	Real flow	Experimental Method
Deniz and Staubli [114]	Rectangular and octagonal cylinders	Real flow	Experimental Method
Masoudi at al. [115] and Masoudi at al. [116]	Polygonal cylinder of sides $N = 5$ to 8	Real flow	Large Eddy Simulation
Xu et al. [117]	N-sided polygons	Real flow	Experimental method
Orlando et al. [118]	16-sided polygonal cylinder with certain peculiarities, e.g. round corners, protuberance due to weld bead, cable, duct and external ladder attached with cylinder	Real flow	Experimental Method
Wang et al. ([119])	Polygonal cylinder of side number $N = 3$ to ∞	Real flow	Proper orthogonal decomposition
Zafar and Alam [120]	Square cylinder with rounded corners	Real flow	Numerical Simulation
Xu et al. [147]	Square cylinder	Real flow	Numerical Simulation
Lee et al. [121]	N-sided isotoxal-star shaped polygonal cylinder	Real flow	Numerical Simulation

Park and Wang [122]	Floating polygonal platforms placed inside a polygonal ring	Wave action	Semi-analytical Method
Scolan and Etienne [123]	Rectangular cylinder	Real flow	Karmann–Trefftz transformation and Theodorsen–Garrick transformation
Tian and Wu [128]	Polygonal cylinder with even number of flat edges (N) and one of the vertices facing the free stream	Inviscid flow and viscid flow (low Reynolds number $Re < 200$)	Schwarz-Christoffel mapping
Tian et al. [129]	Polygonal cylinder with odd number of edges and different orientations	Inviscid flow and viscid flow (low Reynolds number $Re < 200$)	Schwarz-Christoffel mapping
Morishita [130]	Regular polygonal cylinders of sharp corners and straight sides for $N = 3, 4$ and 6	Potential flow	Schwarz-Christoffel mapping
Elcrat and Trefethen [131]	Arbitrary polygonal obstacle	Kirchhoff flow	Modified Schwarz-Christoffel integral
Sarma [132]	Polygonal cylinder	Rotational flow	Schwarz-Christoffel mapping
Kim and Kim [133]	Square cylinder	Potential flow	Higher order multipoles
Murad [134]	2-D Concave body, Circular arc and Kidney Shaped body	Inviscid uniform shear flow	Complex variable method

2.5.1 Real Flow around Multiple Polygonal Cylinders

Vijayasree et al. [148] presented the study of flow behaviour and scour formation around bridge piers of polygonal shape in sediment bed. They have considered the piers of oblong, triangular, rectangular, trapezoidal, and lenticular cross sections (see Figure 2.22) in similar flow settings for the comparison of flow field and scour geometry. The upstream scour depth is found maximum in rectangular pier and found minimum in lenticular shaped pier. The mean velocities around different piers are presented and compared with the velocity distribution on flat-bed.

In one of the similar kinds of study, Zhang et al. [137] investigated the influence of different shapes of piers on the flow patterns in river. The rectangular, circular and elliptical piers are considered, those block the river flow and that changes the flow patterns in local areas around the piers.

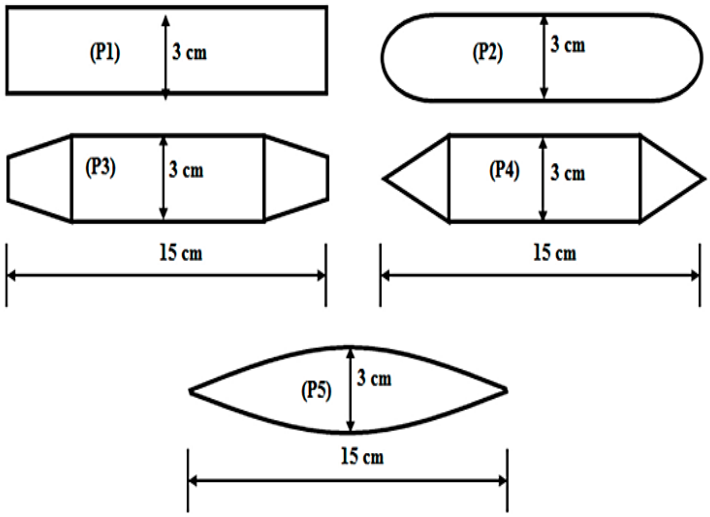

Figure 2.22 (a) Different cross-sectional shapes of piers [148].

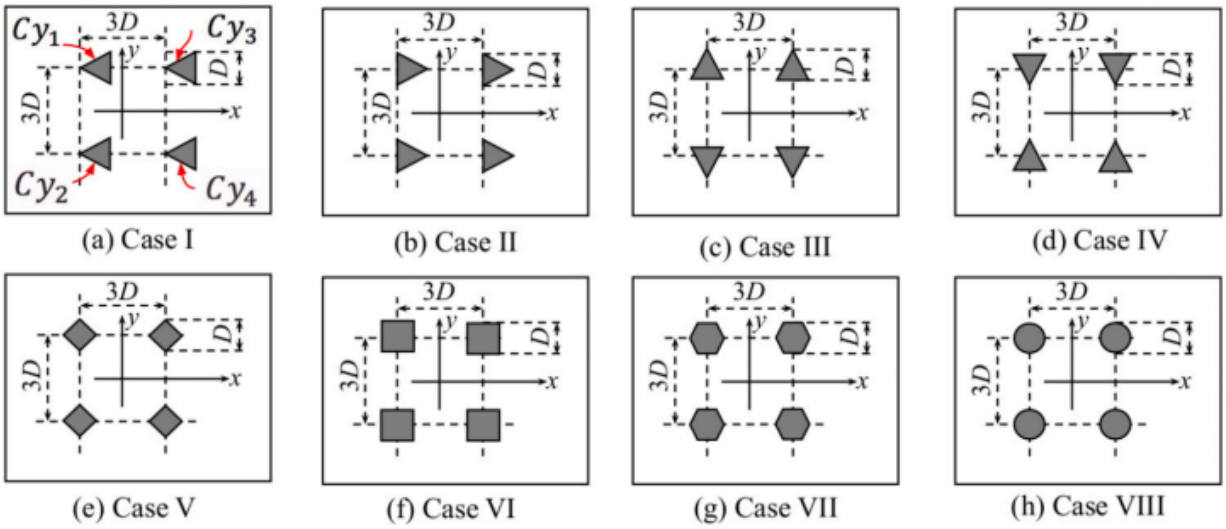

Figure 2.23 Arrangement of four cylinders of different shapes: (a) left triangles, (b) right triangles, (c) up/down triangles, (d) down/up triangles (e) squares rotated 45^0, (f) unrotated squares, (g) regular hexagons, and (h) circles [149].

Fluid flow around a group of four polygonal cylinders of different shapes (e.g. equilateral triangular, square, regular hexagon, and circle cylinders) in square arrangement (Figure 2.23) is investigated numerically using vortex-in-cell method by Nguyen et al. [149]. For cases of left, right, and up/down triangular cylinder in square arrangement, the vortex shedding and, drag and lift forces acting on cylinders are found in synchronous fashion. The magnitudes of hydrodynamic

forces on left oriented triangular cylinders are found less as compared to other orientation of triangular cylinders.

Nouri et al. [150] have conducted numerical simulation using PHOENICS code for flow around single and two polygonal cylinders at Reynolds number $Re = 100$. The cylinders are spaced out by center distances $1.5D$ and $3D$ (where D is the cylinder diameter) in side-by-side and tandem configurations. For single octagonal cylinder, the drag force is reduced by 9.3% as compared to that for circular cylinder. In tandem configuration, the negative drag force is found to act on downstream cylinder, while in side-by-side arrangement of circular cylinders, similar values of drag coefficient are found for both cylinders due to proximity interference between them.

Alam and Zhou [151] have studied the wake past two square cylinders in side-by-side arrangement in real flow of Reynolds number $Re = 300$. The structure and merging patterns of two vortex street are studied, based on that four flow regimes are recognized; the single bluff body regime for $H < 1.2$, the narrow and wide street regime for $1.2 < H < 2.1$, the transition regime for $2.1 < H < 2.4$, and the coupled-street regime for $H > 2.4$. The switching of gap flow is found at two-different time scales known as macro and micro scales. In macro scale, thin jet of flow passing through gap between cylinders remained biased for a long duration and it occurs for $1.2 < H < 2.1$. In micro switch, thick gap flow switches at frequency equal to twice the frequency of vortex shedding. The vortex streets shedding past the cylinder unite to form a single street at certain finite distance downstream. This distance is related to the center distance H between the cylinders by third order polynomial.

The effect of triangular wedge placed in front of circular cylinder on the flow characteristics is investigated by Han et al. [152]. The pressure profile on the surface of circular cylinder for various spacing ratio between wedge and cylinder is shown in Figure 2.24. The pressure distribution becomes uneven with increases of center distance to diameter ratio, that results in drag force acting on the circular cylinder along the direction of flow. The drag and lift force acting on circular cylinder decreases with separation distance for small wedge side length to cylinder diameter ratio (0.20 and 0.27). For larger ratio (0.33 and 0.40), the drag and lift forces experience rise.

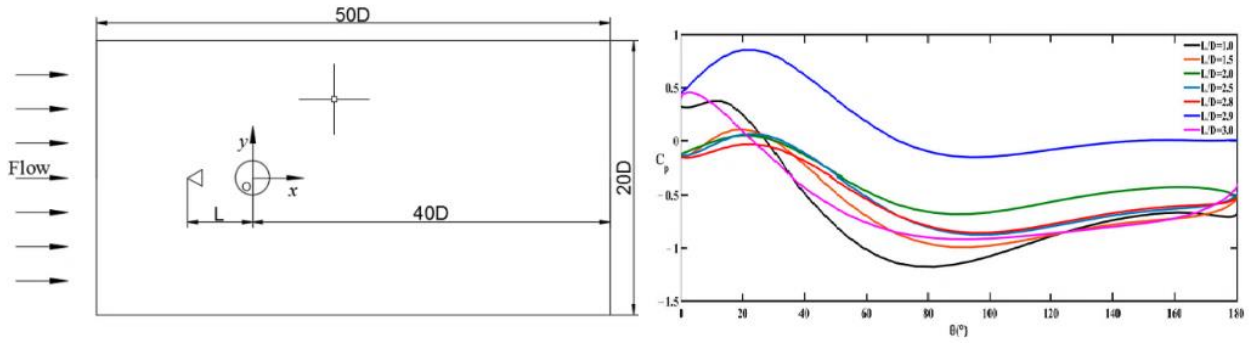

Figure 2.24 (Left) Triangular wedge placed upstream of circular cylinder in fluid flow, (Right) The pressure co-efficient distribution on the surface of circular cylinder for different spacing ratio L/D [152].

Numerical simulation is performed by Wang et al. [153] to investigate flow around two identical trapezoidal cylinders for distance between the cylinders ranging from 0.5 to 10. They considered the effects of cylinder geometry and distance between cylinders on the flow characteristics, flow patterns, and flow instability. It is found that pressure on front side of the upstream trapezoidal cylinder is not significantly affected by spacing between cylinders, and pressure on the upper surface and that on rear surface is significantly affected by the distance between cylinders. Similarly, the pressure on the front side of downstream trapezoidal cylinder attains negative values, and on upper side it is marginally affected by distance between cylinders. The rear surface of downstream cylinder falls in the region of negative pressure of wake behind cylinder.

The hydrodynamic interactions between two freely rotating triangular cylinders in tandem arrangement is examined by Wang [154]. They observed three states of motion, oscillatory rotation for center distance to diameter ratio $H/D = 2$, quasi-periodic autorotation for $H/D = 3$ and, irregular autorotation for $H/D = 4$ and 5. Sohankar et al. [155] studied the flow around two finite length side-by-side square cylinders (Figure 2.25). Following three configurations of cylinders with respect to free stream flow are considered, (1) both cylinders with 0^0incident angle, (2) both cylinders with 45^0 incident angle and, (3) one cylinder with 0^0 angle and other oriented at 45^0 angle. The pressure co-efficient is measured on the surface of both cylinders (across the cylinder and along the length of cylinder) for Reynolds number range 5.9×10^4 to 8.1×10^4.

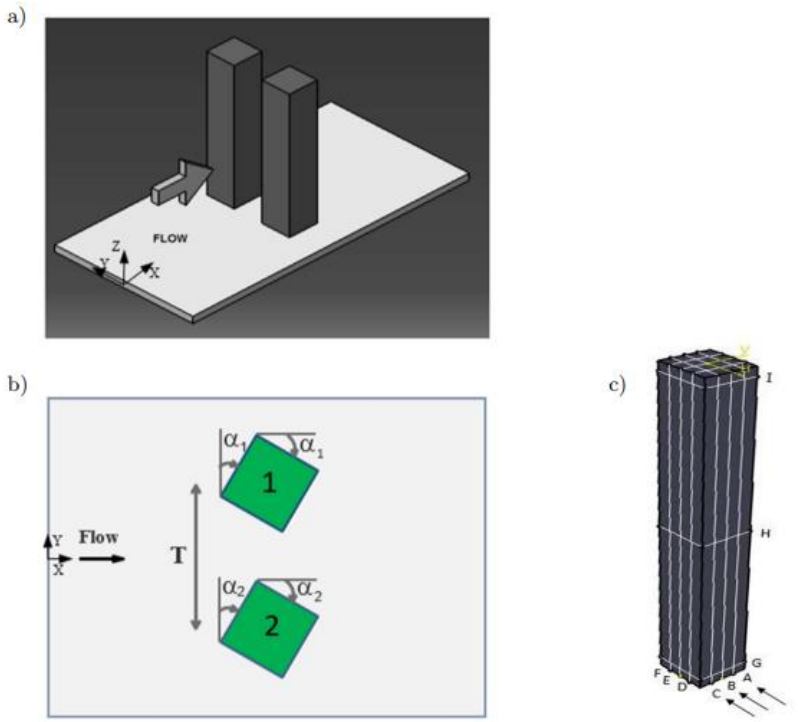

Figure 2.25 Side-by-side configuration of two square cylinders (a) pictorial view (b) two-dimensional view (c) pressure measurement points on the surface of cylinder [155].

Table 2.3 Various types of cylinder geometry, flow conditions and investigation methods used by researcher for flow around pair of cylinders.

Researcher	**Cylinder Geometry**	**Type of Flow Considered**	**Method Used**
Bearman & Wadcock [61], Gao et al. [156], Xu et al. [157]	Pair of circular cylinders	Real flow	Experimental
Weinmann et al.[158], Gopalan and Jaiman [159]	Pair of circular cylinders	Real flow	URANS-Large Eddy Simulation
Derakhshandeh et al. [160]	Pair of circular cylinders	Real flow	Scale Adaptive Simulation
Lin et al. [161]	Pair of circular cylinders	Real flow	FEA and Arbitrary Lagrangian-Eulerian method
Hicks [73]	Pair of circular cylinders	Potential flow	Definite integrals associated with complex velocity potential function
Greenhill [74] and Carpenter [75]	Pair of circular cylinders	Potential flow	Series solution
Huang and Yong [76], Alassar and Ei-Gebeily [77], and Chen et al. [78]	Pair of circular cylinders	Potential flow	Complex variable method and bipolar co-ordinates
Lagally [79]	Pair of circular cylinders	Potential flow	Weierstrass function

Landweber and Shahshahan [162]	Pair of circular cylinders	Motion of cylinders in inviscid flow	Analytical Method
Ahammad and Sen [80]	Pair of circular cylinders	Inviscid flow induced by presence of line source and sink	Earnshaw stream function
Taylor [81]	Pair of circular cylinders	Inviscid oscillatory flow	Bipolar co-ordinate
Wang [82]	Two translating and expanding circular cylinders	Uniform potential flow	Complex variable method (Fourier series expansion)
Borisov et al. [83]	Circular cylinders	Potential flow	Hamiltonian Mechanics
Burton et al. [84]	Two moving circular discs	Potential flow	Complex potentials in terms of first Jacobi theta function
Kawaguti [85]	Two moving circular discs	Potential flow	Method of Images
Bampalas and Graham [86]	Two moving circular discs	Potential flow	Bilinear mapping
Gao et al. [88]	Two unequal circular cylinders	Potential flow	Principle of superposition
Petrov and Maklakov [89]	Ground effect on circular cylinder	Potential flow theory	Complex potential using Jacobi Theta-functions
Baddoo and Ayton [45] and Baddoo et al. [163]	Ground effect on circular cylinder and arc wings	Potential flow theory	Complex potential using P-function
Dalton and Helfinstine [90]	Multiple circular cylinders	Potential flow theory	Method of Images
Crowdy [91]	Multiple circular cylinders	Potential flow theory	Mobius transformation in multiply connected region
DeLillo et al. [92]	Multiple circular cylinders	Potential flow theory	Series solution of potential flow
Sun and Ng [93]	Multiple circular cylinders	Potential flow theory	Complex potential function in form of power series
Vijayasree et al. [148]	Rectangular, oblong, trapezoidal, triangular and lenticular cylinder	Real flow	Experimental Method
Zhang et al. [137]	Rectangular, circular and elliptical	Real flow	Numerical Simulation using MIKE 21 code
Nguyen et al. [149]	Equilateral triangular, square, regular hexagon, and circle cylinders	Real flow	Numerical simulation using Vortex-in-cell method
Nouri et al. [150]	Pair of polygonal cylinders	Real flow	Numerical simulation using PHOENICS code
Alam and Zhou [151]	Pair of square cylinders	Real flow	Experimental Method
Han et al. [152]	Pair of triangular circular cylinder	Real flow	Numerical Simulation
Wang et al. [153]	Pair of trapezoidal cylinders	Real flow	Numerical Simulation
Wang et al. [154]	Two freely rotating triangular cylinders	Real flow	Numerical Simulation

Sohankar et al. [155]	Pair of square cylinders	Real flow	Experimental Method
Chen and Jiangsu [164]	Multiple plates	Potential flow	Fredholm integral equation Solved numerically
Nair and Kanso [165]	Two arbitrary shaped rigid bodies	Potential flow	Kirchhoff potentials
Tchieu et al. [166]	Pair of circular cylinders and two flapping plates	Potential flow	Bilinear mapping and complex potential in form of Laurent's Series
Kadri and Weihs [167]	Two slender bodies	Potential flow	Slender body theory (Asymptotic Technique)
Wnek et al. [168]	Two ships	Potential flow	Panel Method

2.5.2 Potential Flow around Multiple Polygonal Cylinder

Chen and Jiangsu [164] have presented the solution of two-dimensional potential flow around multiple plates. They reduced the problem of potential flow around multiple plates to the system of Fredholm integral equation of second kind. This integral equation is transformed to algebraic form for numerical solution. It is found that the smaller plate influences the flow parameters around the larger plate marginally, while the larger plate has significant influence on the flow around smaller plate.

The hydrodynamic interaction between two arbitrary shaped rigid bodies in potential flow is studied by Nair and Kanso [165] using Kirchhoff potentials. The hydrodynamic coupling between oscillating and free body causes free body to attract towards or repel away from oscillating body. Two attracting bodies due to hydrodynamic coupling starts repelling after certain separation distance and collision is prevented. Such behaviour of drifting body close to two-oscillating bodies is shown in Figure 2.26.

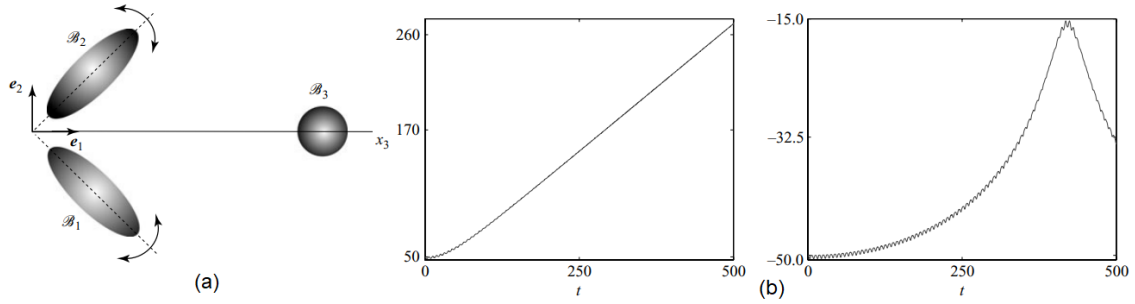

Figure 2.26 (a) A body B_1 and B_2 are forced to oscillate about a hinge at origin of co-ordinate and the body B_3 is free to drift, (b) response of body B_3 driffting away (left) and towards (right) the two oscilolating bodies [165].

Tchieu et al. [166] investigated the hydrodynamic interaction between two circular cylinders using Laurent series expansion and conformal mapping in doubly connected domain. They investigated the interaction between cylinder with prescribed motion and free cylinder. Such interaction is shown in Figure 2.27, where the after cylinder moves under the hydrodynamic forces generated by forward moving cylinder. The velocity of drifting of after cylinder decreases if it is placed in a narrow region behind the moving cylinder. The after cylinder obtains the velocity equal or more then the moving cylinder if it is placed more on the side of forward cylinder's path. This force-free interaction between the cylinders help in understanding the hydrodynamic drifting in aquatic locomotion. They also showed the interaction between two flapping plates. It is observed that for sinusoidal motion of plates in potential flow, the center of two plate system experiences zero hydrodynamic force and torque.

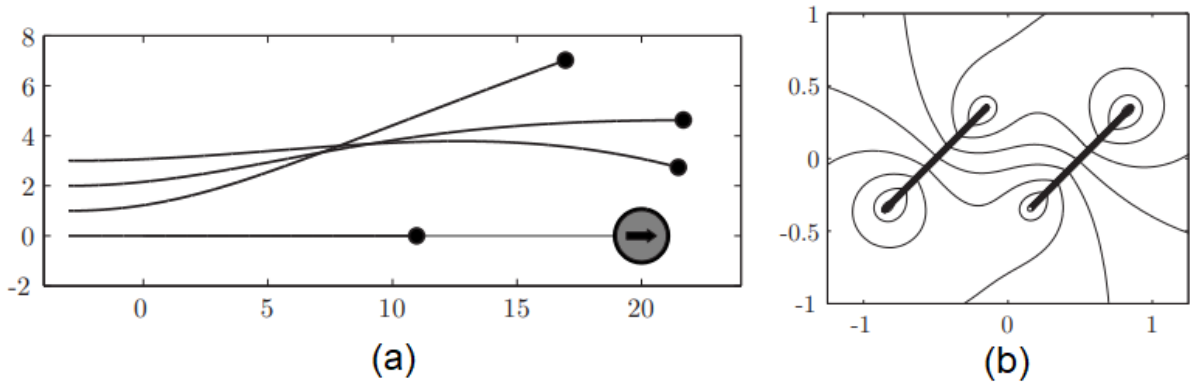

Figure 2.27 (a) Downstream cylinder following the forced motion of upstream cylinder, (b) streamlines around two flapping plates in inviscid fluid [166].

Landweber et al.[162] have studied the interaction between two translating bodies in still inviscid fluid. For the case of moving body approaching towards the stationary body, the equations of motions are derived in Lagrangian form. The added-mass coefficients are obtained using integral-equation procedure for the case of rectangular cylinder approaching a circular cylinder.

The slender body theory is applied by Kadri and Weihs [167] to study the hydrodynamic interaction between two bodies in unbounded potential flow. It is observed that, the forces and moments induced due to hydrodynamic interactions are strongly depend on the separation distance between bodies. The hydrodynamic force acts between two moving bodies (with same velocity) half of the value that acts on the stationary body by the moving one.

The solution of hydrodynamic interaction between two ships in inviscid flow using panel method is carried out by Wnek et al. [168]. The analysis is performed with rigid and deformable free surface. The rigid free surface model underpredicts the magnitude of hydrodynamic forces between the ships for lateral separation distances as compare to that for deformable free surface model. The effects of wave-making are found significant at small separation distances.

Baddoo et al. [163] gave the exact solution for hydrodynamic interaction between wall/ground and wings of various shapes. This study includes various cases of potential flows in doubly connected domain, such as uniform flow, straining flow, and point vortex flow around stationary wing and wing with unsteady motion above the ground. The area above the ground with circular wing, circular arc wing, centered circular arc wing, and flat wing are mapped from an annulus using various conformal maps as shown in Figure 2.28.

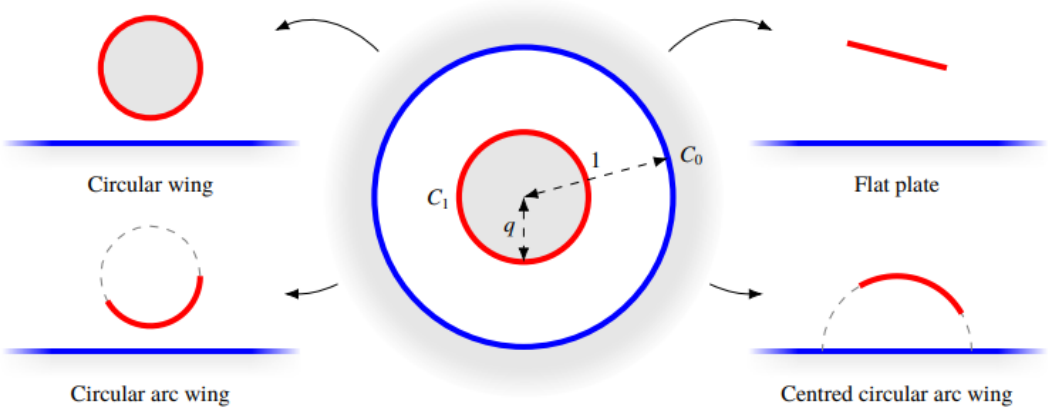

Figure 2.28 Conformal maps from annulus to the wing above the ground. The interior circle C_1 of annulus is mapped to a wing and outer circle C_0 is mapped to ground [163].

2.6 Gaps Identified from Literature Survey

From the literature, it is evident that the interaction between two circular cylinders has gained considerable attention of researchers. However, very few studies have been reported on the flow over interacting polygonal cylinders. Certain parameters in this problem are yet to be discussed and there is lots of scope in improvement of mathematical models, simulation strategies, and solution methodologies. Following are the research gaps identified from literature review.

- The problem of potential flow around single and multiple polygonal cylinders with rounded corners, and hydrodynamic interaction between them in potential flow using complex variable method have yet not been investigated.
- The Schwarz-Christoffel transformation can be employed to generate polygonal geometries with rounded corners, but it is time consuming particularly in multiply connected domain. Therefore, there is severe need to develop mapping function that can handle multiple polygonal geometries at a time.
- A generalized solution that can involve multiple polygonal cylinders in different planar orientation in potential flow condition is not addressed significantly.

2.7 Closing Remark

The detailed literature review on the fluid flow around single and multiple cylinders of circular and polygonal cross-sections is carried out. Various methods and tools used by the researchers for study of fluid flow parameters around the cylinders are mentioned. From the literature review, the research gaps have been identified.